Geol Rundsch (1998) 87: 394–406

ORIGINAL PAPER

R. Hetzel · R. L. Romer · O. Candan · C. W. Passchier

Geology of the Bozdag area, central Menderes massif, SW Turkey: Pan-African basement and Alpine deformation

Received: 4 March 1998/ Accepted: 1 September 1998

Abstract The Menderes massif consists of a Precambrian Core Series that preserves evidence for a polymetamorphic history and a Paleozoic/Mesozoic Cover Series that experienced only the Alpine tectonometamorphic evolution. Structural, petrographic, and geochronologic investigations in the central Menderes massif demonstrate that (a) part of the metamorphic and structural evolution of the Precambrian basement is older than the undeformed 551±1.4-Ma-old Birgi metagranite, and (b) inferred Alpine fabrics overprinting the Cover Series largely have the same attitudes as the old structures in the much older Core Series. The inferred Alpine fabrics include both contractional and extensional structures. Contraction under greenschist to amphibolite facies conditions resulted in the imbrication of the Core and Cover Series and generated an inverted metamorphic sequence by north-directed thrusting. During Alpine extension, most of the south-dipping thrust faults were reactivated as extensional shear zones under decreasing greenschist facies conditions.

Key words Pan-African orogeny · U–Pb dating · Ductile deformation · Shear sense indicators · Menderes massif · Turkey · Thrusting

R. Hetzel (✉) · R. L. Romer
GeoForschungsZentrum (GFZ) Potsdam, Telegrafenberg,
D-14473 Potsdam, Germany

O. Candan
Department of Geological Engineering, Dokuz Eylül University,
TR-35100 Bornova, Izmir, Turkey

C. W. Passchier
Institut für Geowissenschaften, Johannes Gutenberg-Universität,
D-55099 Mainz, Germany

Introduction

The Menderes massif consists of a Precambrian Core Series and a Paleozoic/Mesozoic Cover Series that are characterized by regionally developed foliations and stretching lineations with similar orientation and structural style. As structures in the young Cover Series apparently can be followed into the old Core Series, it has been argued that a dominant phase of Alpine deformation and metamorphism destroyed most traces of the pre-Alpine evolution of the Menderes massif (e.g., Akkök 1983; Sengör et al. 1984). In addition to the formation of a dominant fabric, thrusting in the Central Menderes massif imbricated the Cover Series with the Core Series and formed an inverted metamorphic sequence with metamorphic grade increasing from greenschist to amphibolite facies (Hetzel 1995). Late Alpine structures include large-scale extensional shear zones in the Cover and Core Series (Hetzel et al. 1995a). One extensional shear zone has been intruded by two syntectonic Miocene granodiorites (Hetzel et al. 1995b).

This paper describes contractional structures of inferred Alpine age and distinguishes them from younger extensional structures using contrasts in metamorphic grade and kinematics. A metamorphosed but largely undeformed granite from the Core Series, which cross-cuts structures in the Core Series, has been dated by the U–Pb method on zircon. Instead of an expected Alpine age, the dating yielded a Pan-African age, which demonstrates that (a) the early deformation history in the surrounding Core Series gneisses has a Pan-African age, and (b) structures associated with the Alpine contraction and the Pan-African event are similar in style and orientation and cannot be distinguished everywhere.

Geological setting

The Menderes massif forms a 200x300-km-large culmination of metamorphic rocks in southwestern Turkey. It is located between the Izmir-Ankara Mélange, a Neo-Tethyan suture zone of Cretaceous–Paleocene age, and the Permian–Eocene Lycian nappe complex that roots in this suture zone (Fig. 1; Sengör and Yilmaz 1981; Dora et al. 1990; Collins and Robertson 1997). Lithostratigraphic correlations between Greece and Turkey have been interpreted to indicate that the Menderes massif is the eastward continuation of the Attic Cycladic crystalline complex in the Aegean Sea into mainland Turkey (Dürr et al. 1978; Fig. 1a). The Menderes massif consists of three submassifs (northern, central, and southern) separated by two east-west-trending graben, the Gediz and the Büyük Menderes graben (Fig. 1b).

The Menderes massif has been subdivided in two major tectonometamorphic units, a Precambrian–Cambrian? Core Series and an Ordovician?–Cretaceous Cover Series (Dürr 1975; Sengör et al. 1984; Dora et al. 1995). The Core Series consists of granitic augen gneisses, paragneisses, schists, and minor migmatites. It experienced a polyphase, poorly resolved tectonometamorphic history (Dora et al. 1990, 1995). The oldest clearly documented geological event in the Core Series is the intrusion of large volumes of granites at ~550 Ma in the southern and central submassif (Reischmann et al. 1991; Loos and Reischmann 1995; Hetzel and Reischmann 1996; this study). These intrusions are presumably related to a Pan-African orogeny and most of them were subsequently transformed to augen gneisses (Sengör et al. 1984; Dora et al. 1995). Zircon evaporation ages from granitoid gneisses ranging from 2555 to 1740 Ma and 1000 to 700 Ma, which have been interpreted as intrusion ages (Reischmann et al. 1991), indicate that there are at least two different groups of gneisses. In several localities, small metagabbro/metatonalite bodies in Core Series augen gneisses preserve granulite- and eclogite-facies mineral assemblages of uncertain age (Candan 1995; Oberhänsli et al. 1997).

The local presence of a metaconglomerate in the southern Menderes massif that contains pebbles presumably derived from the Core Series suggests that the Paleozoic/Mesozoic Cover Series has been deposited unconformably on the Core Series (Dora et al. 1995). The lower part of the Cover Series consists of low- to medium-grade schists, phyllites, and quartzites, whereas the upper part is dominated by marbles (Dürr 1975). Metaconglomerates in the southern and central submassif suggest the presence of another unconformity between the lower and upper part of the Cover Series (Dora et al. 1995).

In some places, the simple Core/Cover scheme does not hold and requires modification. For example, metasediments at the southern rim of the Menderes massif that are commonly interpreted as Cover Series have been intruded by augen gneisses dated at 546±1.2 Ma (Hetzel and Reischmann 1996). This indicates that the lower part of the metasedimentary succession in the southern submassif is of Precambrian age. Furthermore, the Core Series in the central Menderes massif occurs structurally above the Cover Series (see Fig. 1 in Dora et al. 1995), which implies that the original Core/Cover relation was disturbed by later thrusting. The importance of nappe stacking during the evolution of the central and southern Menderes massif has recently been emphasized by two other working groups (Gessner et al. 1998; Partzsch et al. 1998).

The Core and the lower part of the Cover Series have together experienced two phases of deformation and metamorphism: a Triassic phase and an Alpine phase. The poorly documented Triassic episode with greenschist facies metamorphic conditions has been suggested for the eastern part of the central submassif (Derbent area; Fig. 1b; Akkök 1983). This phase was followed by the intrusion of the post-tectonic Late Triassic Dede Dagi granite (Dora et al. 1995). Intrusions of similar age are present in the northern submassif (C. Dannat, pers. commun.). The Alpine phase affected the entire Menderes massif and reached upper greenschist to upper amphibolite facies conditions (Akkök 1983; Evirgen and Ashworth 1984; Ashworth and Evirgen 1984, 1985a, b). Regionally distributed Rb/Sr muscovite and biotite ages poorly constrain the Alpine metamorphism of Pan-African gneisses (Satir and Friedrichsen 1986). The maximum age for the Alpine metamorphism is constrained by Cretaceous rudist-bearing marbles that occur at the southern margin of the Menderes massif (Dürr 1975).

Lithotectonic units in the study area

The study area is located in the central submassif of the Menderes massif (Fig. 1b). The Cover Series in the northern part of the study area (Fig. 2) is separated from the Core Series, which dominates in the southern part, by a major south-dipping thrust fault that has been reactivated by ductile and brittle normal faulting. There are two exceptions with respect to the spatial distribution of the Core and Cover Series to the north and south of the major thrust. In the northeastern part of the study area, two small klippen of Core Series rocks rest on a detachment fault. In the southern part of the study area, a slice of Cover Series rocks is tectonically intercalated with Core Series gneisses (Fig. 2). In general, the assemblage chlorite+muscovite±biotite± garnet points to greenschist facies conditions in the Cover Series (Hetzel et al. 1995b). However, the mineral assemblage kyanite, garnet, staurolite, and white mica indicates amphibolite facies conditions in the tectonic slice of Cover Series rocks (Hetzel 1995).

In the Core Series the following lithotectonic units have been distinguished (Fig. 2): (a) Boz Dag schist (after Boz Dag Mountain, the highest peak of the Menderes massif); (b) pelitic gneiss (in part migmatitic); (c) garnet-bearing augen gneiss with lenses of metagabbro (Birgi augen gneiss);

Fig. 1 **a** Map of the Aegean region situated in the backarc of the active Hellenic subduction zone. Map shows the location of the Menderes massif in western Turkey and the Attic Cycladic crystalline complex in the Aegean Sea (after Dürr et al. 1978). **b** Map of the Menderes massif (after Dora et al. 1990) with location of the study area in the central submassif

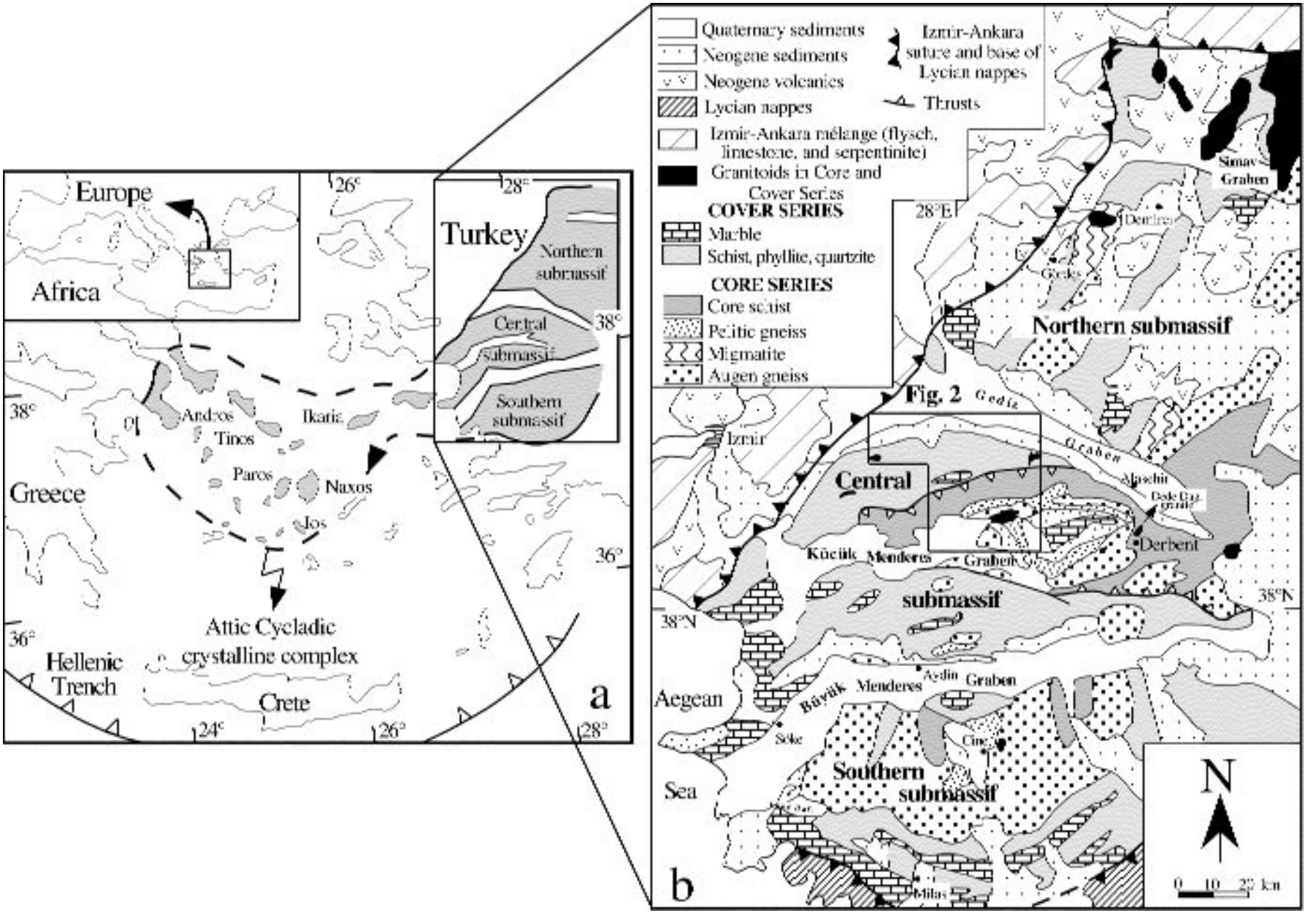
Europe
Africa
Turkey
Northern submassif
Central submassif
Southern submassif
Greece
Andros
Tinos
Ikaria
Paros
Naxos
Jos
Attic Cycladic crystalline complex
Hellenic Trench
Crete
Aegean Sea
a
b
Quaternary sediments
Neogene sediments
Neogene volcanics
Lycian nappes
Izmir-Ankara mélange (flysch, limestone, and serpentinite)
Granitoids in Core and Cover Series
Izmir-Ankara suture and base of Lycian nappes
Thrusts
COVER SERIES
Marble
Schist, phyllite, quartzite
CORE SERIES
Core schist
Pelitic gneiss
Migmatite
Augen gneiss
Fig. 2
Izmir
Gediz Graben
Central submassif
Northern submassif
Simav Graben
Demirci
Gediz
Alaşehir
Derbent
Küçük Menderes Graben
Menderes
Büyük Menderes
Aydın Graben
Söke
Çine
Southern submassif
Milas
N
0 10 20 km

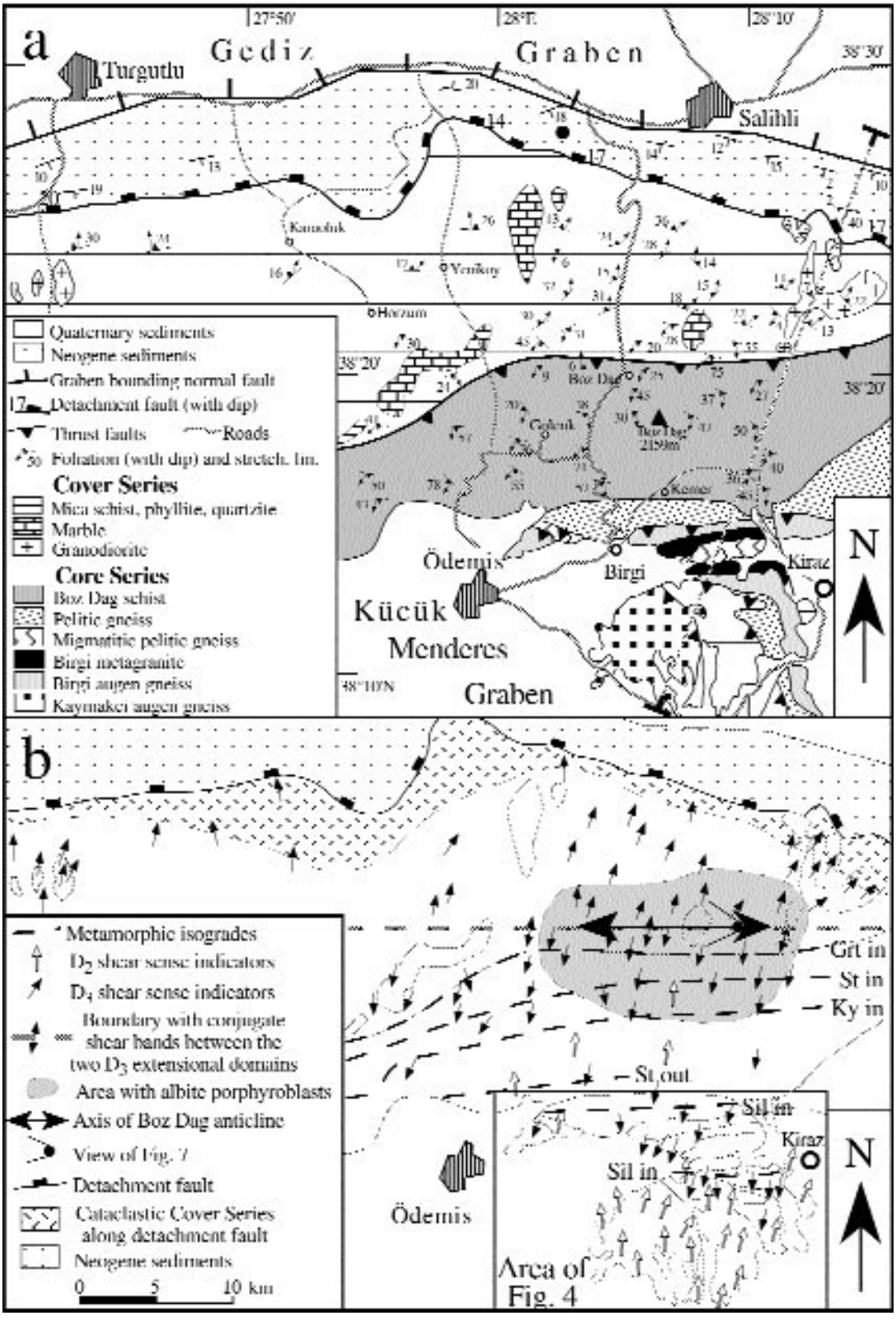
a
Gediz
Graben
Turgutlu
Salihli
27°50'
28°E
28°10'
38°30'
38°20'
Kemalık
Yeniköy
Horzum
Boz Dag
Gelenk
Ikiz Tepe
2159m
Kemer
Ödemis
Birgi
Kiraz
Kücük
Menderes
Graben
38°10'N
N
Quaternary sediments
Neogene sediments
Graben bounding normal fault
Detachment fault (with dip)
Thrust faults
Roads
Foliation (with dip) and stretch. lin.
Cover Series
Mica schist, phyllite, quartzite
Marble
Granodiorite
Core Series
Boz Dag schist
Pelitic gneiss
Migmatitic pelitic gneiss
Birgi metagranite
Birgi augen gneiss
Kaymakci augen gneiss
b
Metamorphic isograds
D2 shear sense indicators
D4 shear sense indicators
Boundary with conjugate shear bands between the two D3 extensional domains
Area with albite porphyroblasts
Axis of Boz Dag anticline
View of Fig. 7
Detachment fault
Cataclastic Cover Series along detachment fault
Neogene sediments
0 5 10 km
Grt in
St in
Ky in
St out
Sil in
Sil in
Kiraz
Ödemis
Area of Fig. 4
N

(d) augen gneiss without garnet (Kaymakci augen gneiss); and (e) a metamorphosed granite (Birgi metagranite).

The Boz Dag schist is distinguished from the Cover Series by the occurrence of amphibolites and the absence of intercalated marble and quartzite. Biotite, kyanite, staurolite, and minor muscovite define a foliation in the Boz Dag schist; in addition, there are garnet, K-feldspar, plagioclase, quartz, and retrograde chlorite. Garnet commonly shows an inclusion-rich core surrounded by an inclusion-free rim that formed at the expense of biotite. Locally, sigmoidal inclusion trails of quartz and graphite indicate a synkinematic growth of garnet. Within the Boz Dag schist, the metamorphic grade increases southwards through a garnet zone, a staurolite-garnet zone, and a kyanite–staurolite–garnet zone (Fig. 2; Izdar 1971; Evirgen and Ashworth 1984). The Boz Dag schist contains amphibolite lenses with hornblende, plagioclase ($An_{27–55}$), garnet, and quartz (Dora et al. 1990). In these lenses, garnet is commonly surrounded by rims of plagioclase, which are locally deformed to platy aggregates. Together with the preferred orientation of hornblende, the deformed plagioclase rims define a weak foliation oriented parallel to the foliation of the host rock of the amphibolite lenses.

The pelitic gneiss consists of quartz, K-feldspar, significant amounts of biotite and garnet, and minor plagioclase and sillimanite. Textural relationships indicate that garnet has formed at the expense of biotite (Hetzel 1995), whereas fibrolitic sillimanite locally replaces biotite and occurs along feldspar grain boundaries (Candan and Kun 1991). The foliation is defined by fine-grained biotite and quartz–feldspar layers alternating with biotite–garnet layers. Where present, a stretching lineation is composed of biotite and quartz/feldspar stringers. Deformed pegmatites in the pelitic gneiss show the same foliation as the gneiss. Migmatitic fabrics with granitic veins and dykes occur between the two bands of the Birgi metagranite (see below; Fig. 2). Where present, the foliation in this migmatitic part of the pelitic gneiss is defined by sillimanite, biotite, feldspars with recrystallized mantles, and quartz layers (Fig. 3a).

The granitic Birgi augen gneiss is everywhere spatially associated with the pelitic gneiss (Fig. 2). It contains biotite, plagioclase, K-feldspar, quartz, garnet, and sillimanite. Coarse-grained weakly deformed parts alternate with finer-grained parts rich in recrystallized biotite and feldspar. Metagabbro lenses in the Birgi augen gneiss (Fig. 4)

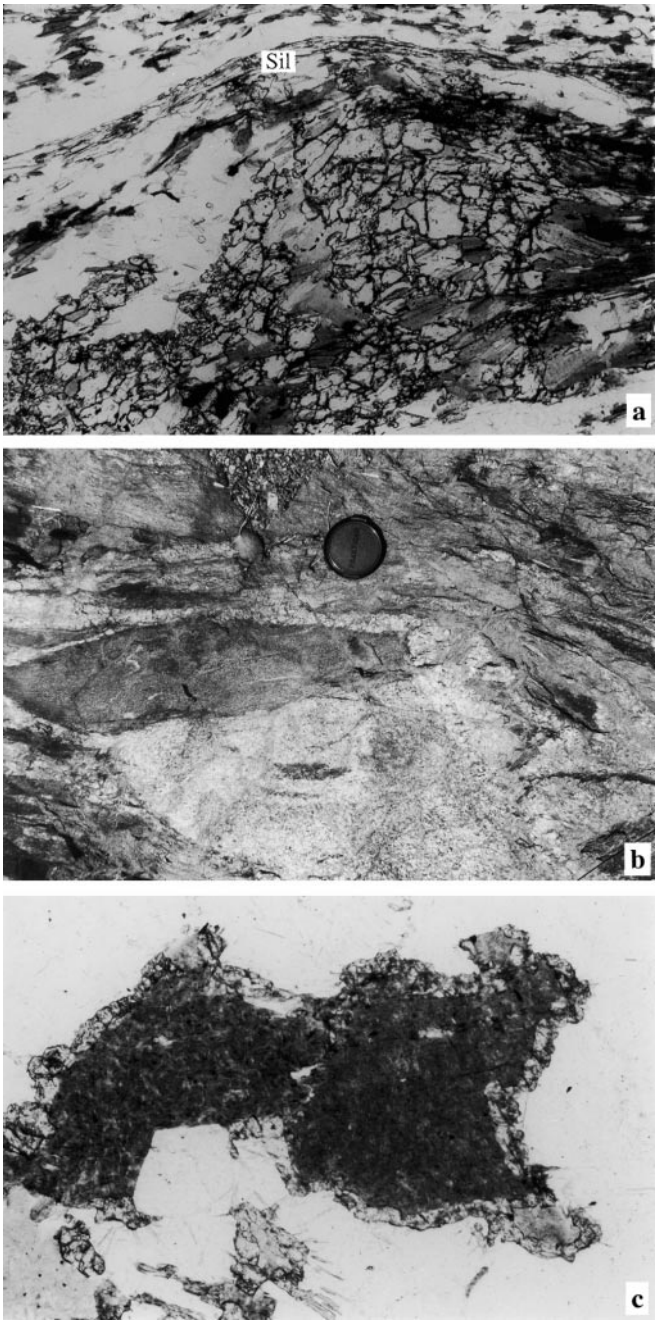

Fig. 3 **a** Migmatitic pelitic gneiss with a foliation defined by sillimanite (Sil) and biotite. Garnet has formed at the expense of biotite. Width of photomicrograph is 3 mm. **b** Intrusive relationship of the Birgi metagranite with the foliated pelitic gneiss. Granite dyke containing a dark, foliated xenolith cross-cuts the foliation of the pelitic gneiss (*right side* of photograph). *Object* for scale is 5 cm in diameter. Location of photograph indicated in Fig. 4 by *asterisk*. **c** Garnet corona around magmatic biotite from the Birgi metagranite demonstrates the metamorphic overprint of the granite. Width of photomicrograph is 1.4 mm

Fig. 2 **a** Map of the study area. Location of the map is shown in 1b. *Black circle* in Neogene sediments ~8 km west of Salihli shows the location where an Eskihisar sporomorph association has been found indicating a middle Burdigalian to middle Seravallian age (~20–14 Ma; Seyitoglu and Scott 1997). **b** Map of the study area showing the metamorphic isograds and the spatial distribution of shear sense indicators. Metamorphic isograds after Izdar (1971), Evirgen and Asworth (1984), Ashworth and Evirgen (1985a, b), and own observations. Shear sense indicators are related to D2 (*open arrows*) and D3 (*filled arrows*). *Arrows* indicate the direction of hanging-wall displacement. The density of arrows illustrates the relative abundance of shear sense indicators as observed in the field. Each arrow represents several shear sense observations made at the starting points of the arrows. Note that the east-west-trending boundary between the two D3 extensional domains is trending oblique to the core/cover thrust which coincides with the garnet isograd. For clarity, contacts between different units are shown as *gray lines*. See text for further explanation

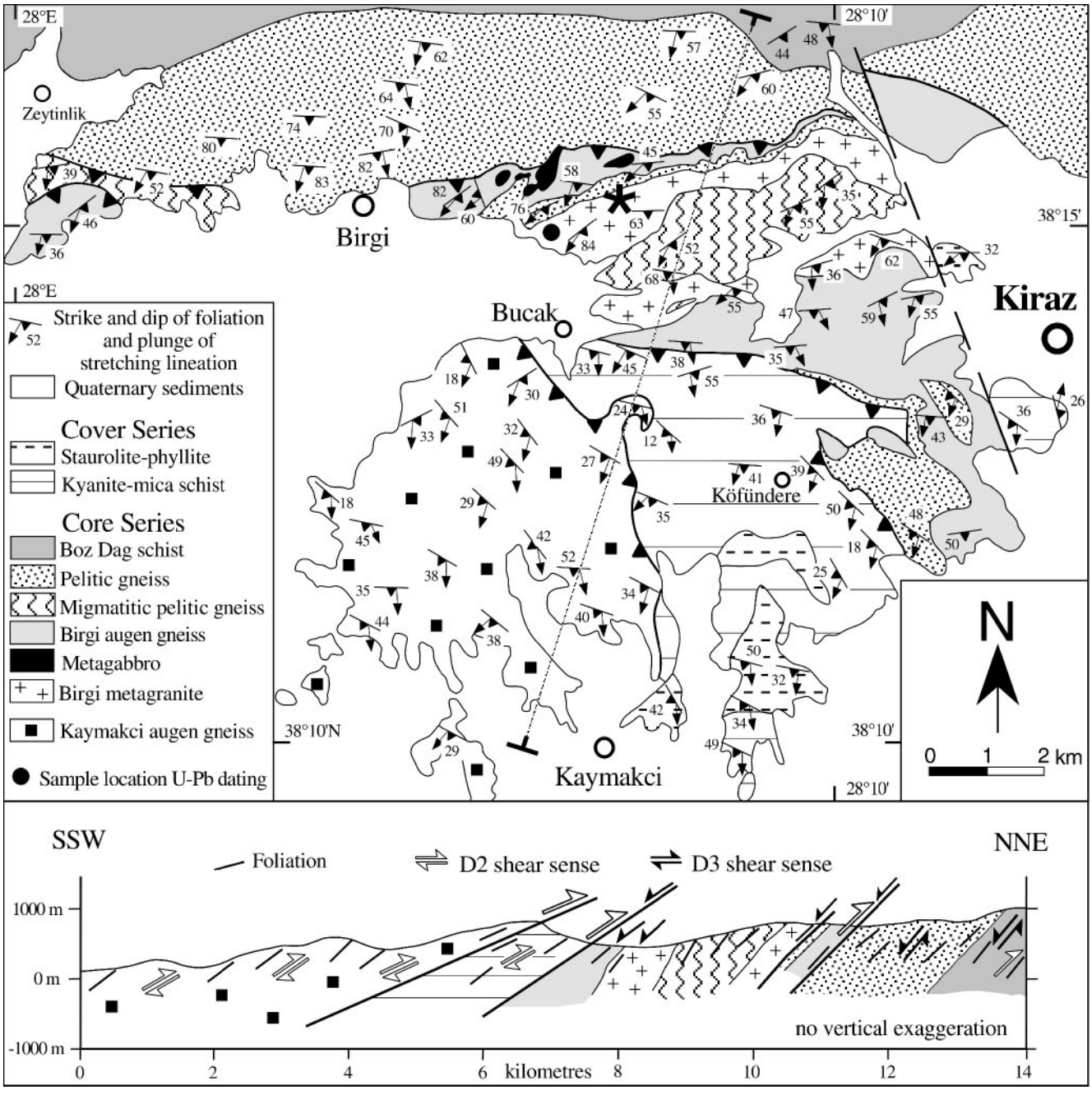

Fig. 4 Map of the Ödemis-Kiraz area (after Candan and Kun 1991; and own observations). For location of the map see Fig. 2. The location of Fig. 3b is indicated by *asterisk*. The *gray line* indicates the location of the NNE-SSW profile illustrating the different senses of shear related to top-to-the-north thrusting (D2) and subsequent top-to-the-SSW extension (D3). See text for explanation

show relicts of a granulite facies metamorphism in their undeformed interior, whereas their deformed margins are partially transformed to eclogite (Oberhänsli et al. 1997). Monazites from the Birgi augen gneiss yielded an age of 660±62 Ma by electron microprobe dating which has been interpreted to date the granulite facies metamorphic event (Oelsner et al. 1997; F. Oelsner, pers. commun.). Following the granulite and eclogite facies metamorphism, the metagabbros and the augen gneiss have been overprinted under amphibolite facies conditions (Oberhänsli et al. 1997).

The Kaymakci augen gneiss south of Birgi (Fig. 2) lacks garnet and is composed of quartz, K-feldspar, muscovite, minor plagioclase, and biotite. The augen gneiss is homogeneously deformed and shows a well-developed foliation and stretching lineation. Feldspars with recrystallized margins commonly form core and mantle structures suggesting lower amphibolite facies conditions during deformation (e.g., Pryer 1993). Quartz shows polygonal fabrics with relatively straight grain boundaries.

The Birgi metagranite constitutes two belts north and south of the migmatitic pelitic gneiss suggesting that migmatization and granite emplacement are related. Along its northern contact, the Birgi metagranite locally has an intrusive relationship and cross-cuts the foliation of the pelitic gneiss, indicating that in part the deformation in the pelitic gneiss is older than the granite (Fig. 3b). Parts of the northern contact show a tectonic foliation that has been reactivated by steeply south-dipping normal faults. Due to poor exposure, a contact relationship of the Birgi metagranite with the Birgi augen gneiss has not been observed. The Birgi metagranite consists of quartz, K-feldspar, plagioclase, biotite, sillimanite, garnet, and muscovite. The interior of the granite is undeformed and igneous textures are commonly preserved. Garnet coronas around magmatic biotite (Fig. 3c) and fibrolitic sillimanite replacing biotite demonstrate that the granite has been metamorphosed; however, there is no evidence for the granulite and eclogite facies events.

U–Pb dating of the Birgi metagranite

The Birgi metagranite is largely undeformed and intruded the deformed pelitic gneiss (Fig. 4). Therefore, it is presumably the youngest unit of the Core Series and provides an important time constraint for the tectonometamorphic evolution of the central Menderes massif. The zircon population from the Birgi metagranite is extremely heterogeneous and includes long-prismatic thin needles and various types of short-prismatic crystals with sharp edges and tips, magmatic or metamorphic corrosion, and metamorphic overgrowth. Needle-shaped zircon has the smallest contribution of inherited zircon and commonly is free of inherited components (Fig. 5a). This type of zircon is interpreted to have crystallized from the granitic magma. Some needles seem to have suffered resorption of edges and tips or to have been overgrown during later metamorphism (Fig. 5b). A few needles with metamorphic overgrowth have distinctive blunt tips. Short prismatic zircon commonly shows various combinations of inherited core with magmatic and metamorphic overgrowth (Fig. 5c).

To determine the crystallization age, three fractions of not abraded, needle-shaped zircon were analyzed. The analytical results are summarized in Table 1 and plotted in a concordia diagram (Fig. 6). Three samples of needle-shaped zircon (1, 2, and 4 in Table 1) define a discordia with an upper intercept at 551.5±1.4 Ma (2σ; MSWD=1.2) that is interpreted as crystallization age of zircon and the granite. The lower intercept is close to the origin of the concordia diagram. Sample 3 consists of rare zircon needles with rounded crystal tips that are typical for zircon

Fig. 5a–c Cathodoluminescence photographs of zircons from the Birgi metagranite. **a** Needle-like long-prismatic magmatic zircon. **b** Magmatic needle-shaped zircon with metamorphic overgrowth along prisma and at top. **c** Short-prismatic magmatic zircon with inherited core. Note rounded tips

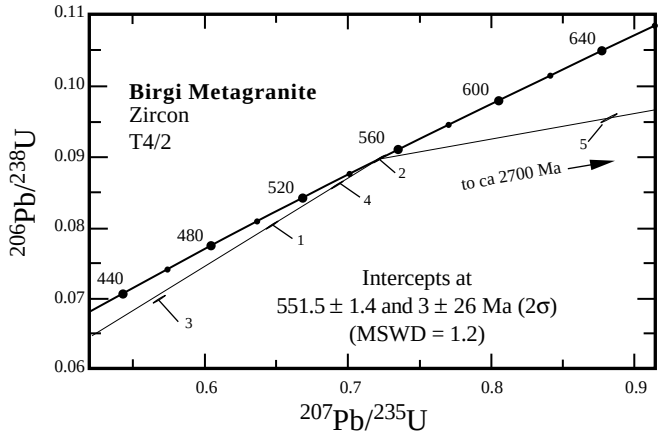

Fig. 6 Concordia diagram for zircons from the Birgi metagranite

with metamorphic overgrowth. This sample is distinctly more discordant than the zircon needles with pointed crystal tips. The higher discordance is interpreted to reflect that the metamorphic overgrowth occurred considerably later than the emplacement of the granite. That the zircon sample with metamorphic overgrowth plots to the right of the discordia defined by samples 1, 2, and 4 indicates that some of the zircon needles contained minor inclusions of inherited zircon. Such minor, optically not recognizable cores in some of the zircon needles has been confirmed by cathodoluminescence. Minor contributions of inherited zircon in the other needles cannot be ruled out. They would shift the lower intercept towards a too young age. Because of this possibility of inheritance, the significance of the lower intercept of the discordia is not completely clear. It could reflect recent lead loss equally well as lead loss during an Alpine metamorphic overprint and crystallization of rims on the zircon needles. Lead loss during an Alpine metamorphic event is preferred as the sample including only zircon with metamorphic tips (sample 3) is the most discordant one (Fig. 6).

Sample 5 consists of short-prismatic zircon with magmatic habitus. Cathodoluminescence shows that this population commonly has inherited cores (Fig. 5c). If these cores are distinctly older than the granite, a discordia through this zircon sample and the emplacement age of the granite would yield an estimate for the average age of the source area of the inherited zircon. Such a discordia indicates that inherited zircon may be as old as 2700 Ma (Fig. 6).

Structural evolution

Overview

In the study area three phases of ductile deformation (D1–D3) have been defined by Hetzel (1995). The presence of granulite- and eclogite facies relics in metagabbro lenses of the Birgi augen gneiss suggests a complex early history with one or more deformation phases, which, for simplicity, are referred to as D1 (see Discussion). D2 fabrics are

Table 1 U–Pb analytical data of zircon from the undeformed pre-Alpine Birgi metagranite, Menderes massif, SW Turkey

Sample[a]	Weight (mg)	Concentrations (ppm)		$\frac{^{206}Pb}{^{204}Pb}$	Radiogenic Pb (%)c			Atomic ratios[c]			Apparent ages (Ma)[d]		
		U	Pb_{tot}	measured ratios[b]	^{206}Pb	^{207}Pb	^{208}Pb	$\frac{^{206}Pb}{^{238}U}$	$\frac{^{207}Pb}{^{235}U}$	$\frac{^{207}Pb}{^{206}Pb}$	$\frac{^{206}Pb}{^{238}U}$	$\frac{^{207}Pb}{^{235}U}$	$\frac{^{207}Pb}{^{206}Pb}$
T4/2													
Common lead $^{206}Pb/^{204}Pb$=17.5±0.1, $^{207}Pb/^{204}Pb$=15.5±0.05, $^{208}Pb/^{204}Pb$=37.5±0.2													
1. (429)	0.425	635	49.3	2105	91.10	5.34	3.56	0.07997	0.64590	0.05858	496	506	552
2. (430)	0.332	828	74.0	1154	91.00	5.34	3.66	0.08970	0.72501	0.05862	554	554	553
3. (478)	0.095	465	30.6	5420	91.54	5.40	3.06	0.06988	0.56796	0.05894	436	457	565
4. (479)	0.167	862	70.2	24170	90.75	5.32	3.93	0.08584	0.69323	0.05857	531	535	551
5. (480)	0.071	891	80.2	16750	90.73	6.12	3.15	0.09486	0.88195	0.06743	584	642	851

[a]Perfectly clear and fracture-free zircon concentrates were obtained using standard mineral separation techniques and separation by hand under the binoculars. No cores were observed under the binoculars but are known from cathodoluminescence studies (cf. Fig. 5). Samples 1, 2, and 4 consist of needle-shaped zircon with distinct edges and tips. Sample 3 includes needle-shaped zircon with rounded and drop-like tips, whereas sample 5 includes only facet-rich short-prismatic grains. All samples were dissolved with 52% HF in Parr autoclaves at 220°C for 4 days, dried, and transferred overnight into chloride form using 6 N HCl at 220°C in the autoclave. Ion-exchange chromatography after aliquotting by weight and tracer addition as described by Krogh (1973)

[b]Lead-isotope ratios corrected for fractionation with 0.1%/a.m.u.

[c]Lead corrected for fractionation, blank, and initial lead. During the measurement period total blanks were less than 15 pg for lead and less than 1 pg for uranium for samples analyzed with a ^{208}Pb–^{235}U mixed tracer

[d]Apparent ages were calculated using the constants of Jaffey et al. (1971) recommended by IUGS (Steiger and Jäger 1977)

Fig. 7 Boz Dag anticline in the Cover Series exposed 5 km north of Boz Dag Mountain. View is towards the west. Note *dark bands* in the hinge and the two limbs of the anticline which consist of mylonitized graphitic quartzite of the Cover Series. The east-west-trending fold axis coincides with the structural boundary between the D3 extensional top-to-the-NNE and top-to-the-SSW shear zones. Location of the photograph is shown in Fig. 2b. See text for explanation

characterized by a synmetamorphic S2 foliation that formed at greenschist to upper amphibolite facies conditions as indicated by synkinematic garnet, staurolite, kyanite or sillimanite, and mica. D3 took place during the retrograde metamorphic evolution and has been interpreted as a result of an Alpine bivergent NNE-SSW-directed extension (Hetzel et al. 1995a). In an ellipsoid-shaped area that coincides with the axial culmination of an east-west-trending anticline (hereafter referred to as Boz Dag anticline; Figs. 2b, 7), post-D2 albite porphyroblasts with straight inclusion trails occur in the Cover Series micaschist and the Boz Dag schist (Hetzel 1995). S3 shear bands postdate albite growth since they curve around or truncate the porphyroblasts (Hetzel et al. 1995a).

Differences between D2 and D3 fabrics in the Ödemis-Kiraz region

D2 structures are best preserved (i.e., least overprinted by D3) in the region between Ödemis and Kiraz, where S2 and S3 foliations dip moderately south to southwest and stretching lineations plunge south to SSW (Fig. 4). The main differences between D2 and D3 fabrics are:

1. D2 fabrics are associated with synkinematic garnet, staurolite, and kyanite, whereas D3 fabrics never contain synkinematic garnet, staurolite or kyanite. Where present in D3 deformation zones, these minerals are prekinematic and have been altered to chlorite.
2. D2 shear bands contain recrystallized biotite, whereas D3 shear bands contain chlorite rather than biotite.
3. D2 fabrics commonly show a polygonal quartz fabric with straight grain boundaries demonstrating either pronounced syntectonic recovery processes and/or posttectonic recrystallization. In contrast, D3 fabrics show bulging of quartz grain boundaries and growth of small new quartz grains indicating dynamic recrystallization.
4. D2 fabrics are characterized by recrystallized feldspar (80–120 μm grain size) that is interpreted to reflect relatively high temperatures during deformation and/or some degree of posttectonic recrystallization. In contrast, recrystallized feldspar in D3 fabrics, associated with fine-grained muscovite, has a smaller grain size (20–50 μm) indicating lower temperatures during deformation and/or the absence of posttectonic recrystallization (Hetzel 1995).
5. Consistently D2 fabric elements include kinematic indicators that demonstrate a top-to-the-north sense of shear, whereas shear sense indicators associated with D3 fabrics indicate a top-to-the-south to SSW shear sense.

Shear sense indicators related to D2 and D3

In the southernmost part of the study area, abundant shear sense indicators demonstrate a top-to-the-north shear sense for D2 (Figs. 2, 4). Top-to-the-north kinematic indicators in the Kaymakci augen gneiss (Fig. 4) include σ-type feldspar clasts (Fig. 8a; cf. Passchier and Simpson 1986) and oblique grain-shape fabrics in quartz (cf. Means 1981). In the cover rocks top-to-the-north asymmetric extensional shear bands (Fig. 8b; cf. Platt and Vissers 1980) and asymmetric decimeter-scale quartz boudins occur (Fig. 8c). Further north, S–C fabrics in the migmatitic pelitic gneiss and sigmoidal inclusion trails in garnet in the Boz Dag schist reveal the same sense of shear.

North of a line joining Kiraz and Bucak almost exclusively D3 top-to-the-south to SSW kinematic indicators are present (Fig. 4). D3 shear bands in the kyanite-bearing schist of the Cover Series occur at the east-west-trending contact with the Birgi augen gneiss. In the Birgi augen gneiss, D3 shear bands and σ-type feldspar clasts are present east of Kiraz. D3 shear bands also occur in the

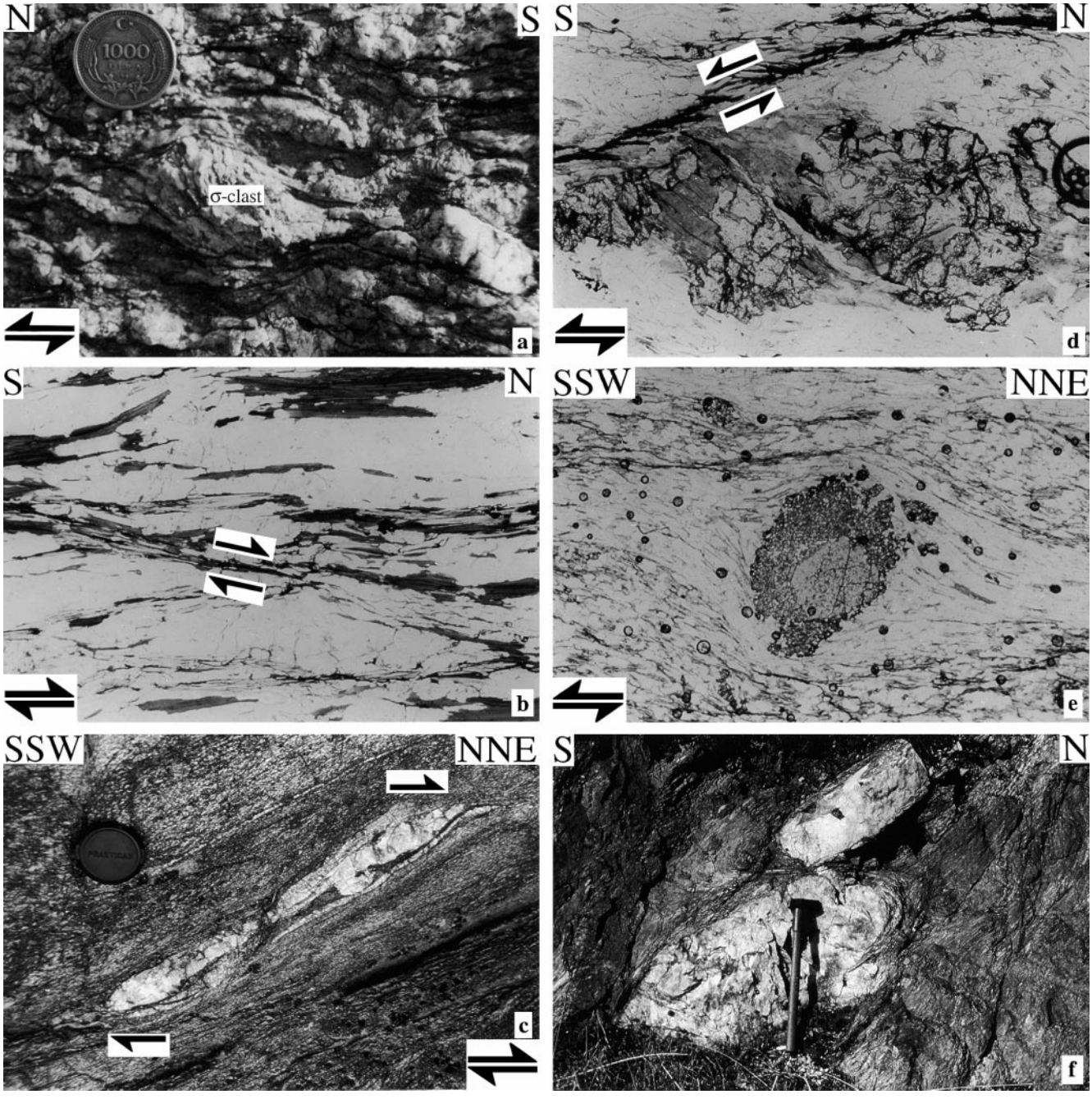

Fig. 8 **a** σ-type feldspar clast in the coherent augen gneiss unit without garnet indicating a top-to-the-north shear sense related to D2. XZ section. *Coin* is ~3 cm in diameter. **b** D2 shear band in the kyanite–-micaschist containing biotite and minor muscovite. Shear band indicates a top-to-the-north shear sense. XZ section. Width of photomicrograph is 6 mm. Plane-polarized light. **c** Asymmetric quartz boudins in the kyanite–micaschist indicating a top-to-the-NNE shear sense related to D2. River section 500 m NE of Köfündere (Fig. 4). XZ section. *Object* for scale is ~5 cm in diameter. **d** Shear band in the migmatitic pelitic gneiss containing chlorite and iron oxides indicates a top-to-the-south shear sense related to D3. Shear band curves around garnet which has formed at the expense of biotite during the prograde metamorphic evolution. XZ section. Width of photomicrograph is 1.4 mm. Plane-polarized light. **e** Asymmetric quartz pressure shadows around garnet in the pelitic gneiss indicating a top-to-the-SSW shear sense related to D3. Fine-grained mineral flakes defining S3 are chlorite. Garnet is interpreted to be pretectonic with respect to D3 and shows an inclusion-free core surrounded by an inclusion-rich rim. The core is probably pre-Alpine, whereas the rim is interpreted to be a result of the Alpine metamorphism during D2. *Dark spots* are air bubbles. XZ section. Width of photomicrograph is 6 mm. Plane-polarized light. **f** Two quartz boudins in the Birgi augen gneiss 2 km south of Zeytinlik (see Fig. 4) indicating the presence of two deformation phases. Boudinage is interpreted to be the result of top-to-the-north shearing (D2), whereas top-to-the-south (D3) shearing brought the boudins into contact again. Close to the boudins S2 has been folded during D3. However, only a few meters away from the boudins no evidence for two distinct phases of deformation is found, i.e., apparently only one foliation and one stretching lineation is present in the rock. XZ section. *Hammer* is ~70 cm long

migmatitic pelitic gneiss (Fig. 8d) and the sheared northern margin of the Birgi metagranite. Further north, asymmetric quartz pressure shadows around garnet have been observed in the pelitic gneiss (Fig. 8e).

As no folding of the older S2 foliation has been observed, it is likely that S2 was in the extension field during D3. This explains why many rocks apparently have only one deformation fabric (i.e., one foliation and one stretching lineation), although the rocks have experienced at least two phases of deformation. These complexities are illustrated in the Birgi augen gneiss where two meter-scale quartz boudins generated during D2 were brought into contact again by D3 (Fig. 8f).

Discussion

The Pre-Alpine evolution

U–Pb dating of magmatic zircons yields an age at 551.5±1.4 Ma for the intrusion of the Birgi metagranite and the migmatites related with this granite. Due to the intrusive relationships of the Birgi metagranite with the foliated pelitic gneiss, the latter unit must be older than 551 Ma. The poorly exposed contact between the Birgi metagranite and the Birgi augen gneiss is also interpreted as intrusive since the Birgi augen gneiss must be older than the granite as shown by its polymetamorphic history (see below). The early deformation history of the pelitic gneiss and the Birgi augen gneiss, here referred to as D1, also predates the Birgi metagranite. This is demonstrated by the relics of granulite and eclogite facies metamorphic minerals in metagabbro lenses in the Birgi augen gneiss (Oberhänsli et al. 1997). Such relics are not present in the Birgi metagranite. The age of this granulite facies metamorphism is interpreted to be given by the monazite chemical age of 660±62 Ma from the Birgi augen gneiss (F. Oelsner et al. 1997; pers. commun.). This suggests that (a) the granulite facies event is older than the Birgi metagranite, and (b) the Birgi augen gneiss is significantly older than other augen gneisses in the Menderes massif which have been dated at ~550 Ma (Loos and Reischmann 1995; Hetzel and Reischmann 1996). With the presently available data the complex early evolution in the Birgi augen gneiss, including the metagabbros and the pelitic gneiss, cannot be better resolved.

The widespread replacement of biotite by garnet in the Core Series and the Birgi metagranite is related to a younger amphibolite facies metamorphic event that is closely associated with the D2 top-to-the-north fabrics. This tectonometamorphic event could be related to a late stage of the Pan-African evolution, the Triassic stage of magmatism and metamorphism, or the Alpine orogeny. A relation of this tectonometamorphic event with a late stage of the Pan-African evolution is favored by the apparent lack of prograde replacement of biotite by garnet in Cover Series, but seems barely compatible with the similarity and coherence in structural style in both the Core and Cover Series. A Triassic age for this event is unlikely as it is in conflict with the observations of Akkök (1983) that the Triassic metamorphism did not exceed greenschist facies conditions. With the presently available data, an Alpine age is likely for this tectonometamorphic event since it would agree with the coherence in structural style and the presence of the D2 top-to-the-north kinematic indicators in both, the Core and Cover Series. The absence of the reaction biotite-to-garnet in the Cover Series may be due to lower metamorphic conditions attained in the Cover Series.

The post-D1 tectonometamorphic evolution

Since D2 resulted in the imbrication of the Core and Cover Series and metamorphism of the Cover Series, we suggest that D2 is the result of Alpine crustal thickening. Synmetamorphic top-to-the-north shear sense indicators suggest that ductile north-directed thrusting resulted in the imbrication and the stacking of the Core and Cover Series units and their internal deformation under greenschist to amphibolite facies conditions. The northward transport of the Birgi augen gneiss during D2 is reflected by the presence of two augen gneiss klippen above the detachment fault (Figs. 2, 9). The klippen are in strong contrast to the underlying greenschist facies cover rocks because they contain eclogite relics characteristic for the Birgi augen gneiss (Dora et al. 1995).

The coincidence of the garnet isograde with the main Core/Cover thrust (Izdar 1971) demonstrates the importance of this major structure. The inverted metamorphic sequence in the Boz Dag schist, defined by the metamorphic isograde and the south-dipping foliation, provides additional evidence for important top-to-the-north shearing (Fig. 2). We interpret the inverted metamorphic sequence as the result of numerous north-directed thrusts within the Boz Dag schist. These thrusts are interpreted to postdate the peak of the Alpine metamorphism and place higher-grade rocks onto lower-grade rocks (Fig. 9). The decrease in metamorphic grade from south to north indicates that thrusting propagated northward with time. Similar scenarios have been suggested for the best-known example of an inverted metamorphic sequence, associated with the Main Central Thrust in the Himalayas (e.g., Treolar et al. 1989; Harrison et al. 1997).

The Boz Dag anticline is the last major feature that formed before D3 extension as shown by the following observations. Since the albite porphyroblasts are restricted to the core of the anticline, the spatial distribution of the pre-D3 albite porphyroblasts is controlled by the anticline; thus, the anticline must have been formed before D3. On the other hand, the anticline postdates the metamorphic isograde defining the inverted metamorphic sequence and is therefore younger than D2 top-to-the-north thrusting.

Crustal thickening was followed by D3 extension that led to a thinning of the previously thickened crust. D3 extension most likely resulted from the high potential energy of the thickened crust and changing plate-boundary conditions along the Hellenic subduction zone, i.e., the roll back

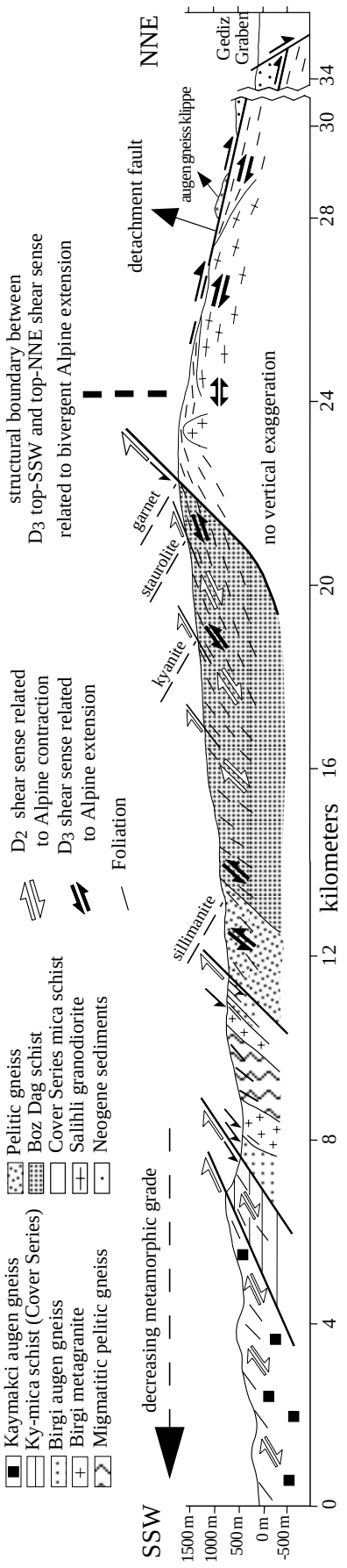

Fig. 9 NNE–SSW cross section through the study area illustrating the different senses of shear related to D2 top-to-the-north thrusting and subsequent D3 top-to-the-SSW extension. Location of cross section is shown in Fig. 2a. The north-directed D2 thrusts responsible for the inverted metamorphic sequence within the Boz Dag schist are illustrated

of the subducting African plate (Hetzel et al. 1995a). D3 extensional fabrics formed under retrograde greenschist facies conditions and have strongly overprinted the D2 fabrics (Fig. 8d). In the Ödemis-Kiraz region most of the D2 thrusts have been reactivated by ductile D3 shear zones (Fig. 4). In the Boz Dag schist and the pelitic Cover Series lithologies further to the north, D3 structures comprise a well-developed shear band cleavage and a pronounced NNE-SSW-directed stretching lineation (Hetzel et al. 1995a).

The Boz Dag anticline had a profound influence on the geometry and the location of the two D3 extensional shear zones which formed along the limbs of the anticline. On the northern limb occur abundant top-to-the-NNE shear sense indicators, whereas on the southern limb top-to-the-SSW shear sense indicators are present, attesting to a bivergent extension (Hetzel et al. 1995a). The top-to-the-NNE extensional shear zone was intruded by two Miocene granodiorites (Fig. 2) with ^{40}Ar–^{39}Ar biotite ages at 12.2 and 13.1 Ma that record exhumation and cooling (Hetzel et al. 1995b). Progressive exhumation resulted in the formation of a north-dipping detachment fault upon which two augen gneiss klippen and syntectonic Neogene sediments were tectonically emplaced (Fig.9). The oldest unmetamorphosed Neogene sediments have a middle Burdigalian to middle Seravallian age (~20–14 Ma; Seyitoglu and Scott 1997). The similar ages of the granodiorites and the Neogene sediments provides evidence for major displacements along the extensional fault system. The widespread occurrence of early Miocene sediments in the graben and basins of the central and northern Menderes massif suggests that D3 extensional faulting started in the early Miocene (Seyitoglu et al. 1992; Seyitoglu and Scott 1992, 1994, 1997).

Acknowledgements We thank C. Johnson for the separation of the zircons from the Birgi metagranite sample. We are grateful to W. Todt and U. Poller from the Geochemistry Department, and J. Huth from the Cosmochemistry Department, of the Max-Planck Institute in Mainz for providing the cathodoluminescence photographs. We would like to thank M. Coté, S. Lin and an anonymous reviewer for constructive and helpful reviews.

References

Akkök R (1983) Structural and metamorphic evolution of the northern part of the Menderes massif: new data from the Derbent area and their implications for the tectonics of the massif. J Geol 91: 342–350

Ashworth JR, Evirgen MM (1984) Garnet and associated minerals in the southern margin of the Menderes massif, southwest Turkey. Geol Mag 121: 323–337

Ashworth JR, Evirgen MM (1985a) Plagioclase relations in pelites, central Menderes massif, Turkey. I. The peristerite gap with coexisting kyanite. J Metamorph Geol 3: 207–218

Ashworth JR, Evirgen MM (1985b) Plagioclase relations in pelites, central Menderes massif, Turkey. II. Perturbation of garnet–plagioclase geobarometers. J Metamorph Geol 3: 219–229

Candan O, Kun N (1991) Possible Pan-African metavolcanics in the Ödemis submassif of the Menderes massif, western Turkey. Min Res Expl Bull 112: 1–16

Candan O (1995) Relicts of granulite-facies metamorphism in the Menderes massif. Turk J Earth Sci 4: 35–55 (in Turkish)

Collins AS, Robertson AHF (1997) Lycian melange, southwestern Turkey: an emplaced Late Cretaceous accretionary complex. Geology 25: 255–258

Dora OÖ, Kun N, Candan O (1990) Metamorphic history and geotectonic evolution of the Menderes massif. Proc Int Earth Sci Coll Aegean Region, pp 102–115

Dora OÖ, Candan O, Dürr S, Oberhänsli R (1995) New evidence on the geotectonic evolution of the Menderes massif. Proc Int Earth Sci Coll Aegean Region, pp 53–72

Dürr S (1975) Über das Alter und geotektonische Stellung des Menderes-Kristallins/SW-Anatolien und seine Äquivalente in der mittleren Ägäis. Habilitation thesis, Marburg, Germany, pp 1–107

Dürr S, Altherr R, Keller J, Okrusch M, Seidel E (1978) The Median Aegean Crystalline belt: stratigraphy, structure, metamorphism, magmatism. In: Cloos H, Roeder D, Schmidt K (eds) Alps, Apennines, Hellenides. Schweizerbart, Stuttgart, pp 455–477

Evirgen MM, Ashworth JR (1984) Andalusitic and kyanitic facies series in the central Menderes massif, Turkey. N Jahrb Min Mh 5: 219–227

Gessner K, Lackmann W, Ring U, Passchier CW, Güngör T (1998) Alpine nordgerichtete Scherung im Menderes Massiv Südwestanatoliens und regionale Konsequenzen. In: Kroner U (ed) Seventh Symposium Tektonik-Strukturgeologie-Kristallingeologie, Freiberg, pp 77–79

Harrison TM, Ryerson FJ, Le Fort P, Yin A, Lovera OM, Catlos EJ (1997) A Late Miocene–Pliocene origin for the Central Himalayan inverted metamorphism. Earth Planet Sci Lett 146: E1–E7

Hetzel R (1995) The Alpine tectono-metamorphic evolution of the central Menderes massif. PhD thesis, Mainz, pp 1–78

Hetzel R, Passchier CW, Ring U, Dora OÖ (1995a) Bivergent extension in orogenic belts: the Menderes massif (SW Turkey). Geology 23: 455–458

Hetzel R, Ring U, Akal C, Troesch M (1995b) Miocene NNE-directed extensional unroofing in the Menderes massif, southwestern Turkey. J Geol Soc Lond 152: 639–654

Hetzel R, Reischmann T (1996) Intrusion age of Pan-African augen gneisses in the southern Menderes massif and the age of cooling after Alpine ductile extensional deformation. Geol Mag 133: 565–572

Izdar E (1971) Introduction to geology and metamorphism of the Menderes massif of western Turkey. In: Campbell AS (ed) Geology and history of Turkey. The Petroleum Exploration Society of Libya, Tripoli, Libya, pp 495–500

Jaffey AH, Flynn KF, Glendenin LE, Bentley WC, Essling AM (1971) Precision measurement of half-lives and specific activities of ^{235}U and ^{238}U. Phys Rev C4: 1889–1906

Loos S, Reischmann T (1995) Geochronological data on the southern Menderes massif, SW Turkey, obtained by single zircon Pb evaporation. Terra Abstr 5: 353, EUG VIII

Means WD (1981) The concept of a steady-state foliation. Tectonophysics 78: 179–199

Oberhänsli R, Candan O, Dora OÖ, Dürr S (1997) Eclogites within the Menderes massif/western Turkey. Lithos 41: 135–150

Oelsner F, Candan O, Oberhänsli R (1997) New evidence for the time of the high-grade metamorphism in the Menderes massif, SW Turkey. Terra Nostra 97 (1): A16

Partzsch JH, Oberhänsli R, Candan O, Warkus FC (1998) The evolution of the central Menderes massif, west Turkey: a complex nappe pile recording 1.0 Ga of geological history. In: Kroner U (ed) Seventh Symposium Tektonik-Strukturgeologie-Kristallingeologie, Freiberg, pp 166–168

Passchier CW, Simpson C (1986) Porphyroclast systems as kinematic indicators. J Struct Geol 8: 831–844

Platt JP, Vissers RLM (1980) Extensional structures in anisotropic rocks. J Struct Geol 4: 397–410

Pryer LL (1993) Microstructures in feldspars from a major crustal thrust zone: the Grenville Front, Ontario, Canada. J Struct Geol 15: 21–36

Reischmann T, Kröner A, Todt W, Dürr S, Sengör AMC (1991) Episodes of crustal growth in the Menderes massif, W Turkey, inferred from zircon dating. Terra abstracts 3: 34, EUG VI

Satir M, Friedrichsen H (1986) The origin and evolution of the Menderes massif, W-Turkey: a rubidium/strontium and oxygen isotope study. Geol Rundsch 75: 703–714

Sengör AMC, Yilmaz Y (1981) Tethyan Evolution of Turkey: a plate tectonic approach. Tectonophysics 75: 181–241

Sengör AMC, Satir M, Akkök R (1984) Timing of tectonic events in the Menderes massif, western Turkey: implications for tectonic evolution and evidence for Pan-African basement in Turkey. Tectonics 3: 693–707

Seyitoglu G, Scott BC, Rundle CC (1992) Timing of Cenozoic extensional tectonics in west Turkey. J Geol Soc Lond 149: 533–538

Seyitoglu G, Scott BC (1992) The age of the Büyük Menderes graben (west Turkey) and its tectonic implications. Geol Mag 129: 239–242

Seyitoglu G, Scott BC (1994) Late Cenozoic basin development in west Turkey: Gördes basin tectonics and sedimentation. Geol Mag 131: 631–637

Seyitoglu G, Scott BC (1997) The age of the Alasehir graben (west Turkey) and its tectonic implications. Geol J 31: 1–11

Steiger RH, Jäger E (1977) Subcommision on geochronology: convention on the use of decay constants in geo- and cosmochronology. Earth Planet Sci Lett 36: 359–362

Treolar PJ, Broughton RD, Williams RP, Coward MP, Windley BF (1989) Deformation, metamorphism and imbrication of the Indian plate south of the Main Mantle thrust. J Metamorph Geol 7: 111–125